Manifestation of granularity in the transport current of coated conductors

M Lao[1,2] , **P Pahlke**[3], **M Sieger**[3], **M Falter**[4], **M Bäcker**[4], **J Hänisch**[2] ,
R Hühne[3] and **M Eisterer**[1]

[1] Atominstitut, TU Wien, Stadionallee 2, A 1020 Vienna, Austria
[2] Institute of Technical Physics, Karlsruhe Institute of Technology, Hermann von Helmholtz Platz 1,
D 76344 Eggenstein Leopoldshafen, Germany
[3] Institute for Metallic Materials, IFW Dresden, Helmholtzstrasse 20, D 01069 Dresden, Germany
[4] Deutsche Nanoschicht GmbH, Heisenbergstrasse 16, D 53359 Rheinbach, Germany

E mail: mayraluna.lao@kit.edu

Abstract

The effects of granularity on the angle and field dependence of the transport J_c in coated conductors (CCs) are discussed. The granularity is revealed by scanning Hall probe microscopy of the trapped field profiles in tapes with different architectures. It was found that pulsed laser deposited (PLD) YBCO film on a RABiTS NiW substrate has the most prominent granular morphology in its trapped field profiles. This is complemented by a peculiar behavior of the critical currents when the orientation of the applied field is within a certain angular range around the ab-planes: $J_c(\theta)$ becomes independent of the angle and $J_c(B)$ exhibits a peak. These phenomena are explained by the physics of Abrikosov Josephson vortices at grain boundaries (GB) that leads to a transition from a GB-limited to a grain-limited regime both in $J_c(\theta)$ and $J_c(B)$. The effects of granularity are strongly suppressed by the chemical solution deposition route for growing YBCO films on NiW, and are almost absent in PLD-YBCO on ABAD-textured templates. These results identify the collective influence of the GB on the percolative current flow in CCs, which becomes most significant at low temperatures.

Keywords: coated conductors, critical current density, granularity

(Some figures may appear in colour only in the online journal)

1. Introduction

High temperature superconductors (HTS) are the best materials known so far for applications that involve the generation of large magnetic fields due to their high current carrying capability, especially if operated at low temperatures. One of the most promising ways to exploit HTS is through the coated conductor (CC) technology. CCs are metallic tapes with a thin coating of a superconducting material belonging to the $RE\mathrm{Ba_2Cu_3O_{7\ \delta}}$ (RE = rare earth, REBCO) family. Due to the crystalline nature of REBCO compounds, the formation of a granular network during its growth is inevitable. Misorientation angles between adjacent grains, θ_{GB}, that are too large have detrimental effects on the overall current carrying capacity since the intergrain J_c decreases exponentially with increasing θ_{GB} beyond a critical angle, θ_c, of about $3°\ 4°$ [1].

Low angle grain boundaries (LAGB) can be described as an array of dislocation cores [2] that start overlapping as θ_{GB} increases, forming a continuous distorted region at high-angle grain boundaries with a Josephson junction-like behavior [3]. Below θ_c, vortices in the LAGBs act like Abrikosov vortices (AV) while the so-called Abrikosov Josephson vortices (AJV) form within a certain range of θ_{GB} and applied magnetic field, H, if the strain fields but not the dislocation cores are overlapping. In-field transport J_c studies on YBCO films on bicrystal substrates have shown that the transport current across grain boundaries (GB) approaches that of the single grains as the field increases, where upon this transition (the so-called cross-over field) depends on the GB angle [1, 4]. This means that the effects of LAGBs on the global J_c is limited to low applied fields. However, as the operation temperature decreases, the field range of the GB limitation increases [5].

Over the years, the properties of CCs went through big improvements by the successful production of CCs with only LAGBs. The improvement has been achieved by using metallic templates with a biaxial texture. Various deposition techniques were implemented with the additional aim of achieving low production costs. Two of the most common methods are pulsed laser deposition (PLD) and chemical solution deposition (CSD). Two types of commercially available templates are typically used: a rolling-assisted biaxially textured substrate (RABiTS) made from NiW alloys and Hastelloy or stainless steel tapes with a textured buffer layer prepared by ion-beam assisted deposition or inclined substrate deposition. Various studies have shown that RABiTS tapes have large grains of usually more than 20 μm, which are transferred to the deposited REBCO layer [2, 6, 7].

Most of the studies to elucidate effects of LAGBs on the current transport used bicrystal substrates, where θ_{GB} can be well controlled and GB effects can be systematically studied. However, not much work was actually devoted to the granularity effects on the transport J_c of CCs, especially at intermediate temperatures, where the GB network acts in a more complex manner. In this work, we report for the first time, peculiar effects of the granular morphology to the transport $J_c(B, T, \theta)$ behavior of tapes with different architectures.

The paper is organized as follows. In section 2, the architecture of the CC samples and the two main characterization techniques   scanning Hall probe microscopy (SHPM) and J_c transport measurements   are briefly described. In sections 3.1 and 3.2, the results on the PLD-grown films and the implication of the strong granularity are assessed by transport measurements. In section 3.3, a peculiar behavior observed in the field dependence of J_c and the mechanism which explains the transition from the GB-limited to the grain-limited regime is discussed. In section 3.4, the investigation is extended to CSD-grown films with different granularity. Finally the conclusions are presented in section 4.

2. Experimental details

Two of the samples investigated in this study are based on RABiTS Ni-5at%W with chemically deposited CeO_2 and $La_2Zr_2O_7$ buffer layers fabricated by Deutsche Nanoschicht GmbH. One of the YBCO films was deposited by PLD at IFW Dresden, the other one by CSD at Deutsche Nanoschicht GmbH and they will be referred to as PLD-NiW and CSD-NiW, respectively. Another sample was investigated for comparison having a PLD-YBCO grown film on stainless steel with textured buffer layers consisting of yttrium-stabilized ZrO_2 prepared by alternating beam assisted deposition (ABAD) and PLD-CeO_2. The ABAD-textured template was produced by Bruker HTS GmbH and this sample is named as PLD-SS.

The spatial homogeneity of the superconducting properties was imaged using SHPM. The setup consists of a Hall effect sensor with a piezo-positioning system [8, 9]. Magnetic field profiles were recorded in a He-gas flow cryostat where the temperature can be stabilized between 3 K and 300 K with

a spatial resolution of 5 μm. A sufficiently large magnetic field oriented orthogonal to the sample surface was applied and consequently reduced to zero to achieve a fully-penetrated state.

Electrical transport properties were measured using the four-probe method in a He-gas flow cryostat equipped with a 5 T split-coil magnet. The direction of the applied field was varied with respect to the main sample axes, and angle-resolved J_c was measured under maximum Lorentz force. All the experimental current voltage characteristics are well-described by a power law relation. J_c was evaluated with an electric field criterion of 1 μV cm^{-1} [1].

For the SHPM measurements, circular areas with a diameter of about 450 μm were patterned by wet chemical etching. Two centimeter-long pieces of the samples with patterned bridges were used for the transport measurements. The PLD-grown tapes have laser-structured bridges [10] with a width of 300 μm and a length of 1 mm while the bridge on CSD-NiW was patterned by wet chemical etching having a width of 250 μm and a length of 2 mm. The thickness of the YBCO layer is about 1.5 μm in all samples.

3. Results and discussion

3.1. Magnetic granularity in PLD-grown films

The remanent field profiles of PLD-SS and PLD-NiW at 5 K presented in figures 1(a) (b) show distinct differences. The trapped field in PLD-SS has a more homogeneous shape than the granular morphology in PLD-NiW. The YBCO film on the ABAD-based template has grains of less than 1 μm in diameter and in-plane θ_{GB} below 3°. As discussed in detail in [6], the formation of magnetic grains is directly correlated to the underlying microstructure of the NiW substrate. The NiW substrate has grains of up to 100 μm. The YBCO film grown can have varying porosity, grooved boundaries and has an average θ_{GB} of up to 10° [7]. The granularity in the profile of PLD-NiW persists up to applied fields of 4 T at 5 K [6] and remains visible in the whole temperature range between 4 K and 77 K as shown in figure 1(c).

3.2. Transport critical current density of PLD-grown films

$J_c(B)$ of PLD-SS (figure 2(a)) decreases monotonically with field for the two main orientations, as expected and widely observed in CCs. On the other hand, PLD-NiW (figure 2(b)) has a peculiar behavior, which leads to two different characteristics when the applied field is oriented either parallel to the *ab*-planes or to the *c*-axis. At small applied fields, J_c does not change systematically but scatters stochastically around its zero field value in both orientations. After a small field range, a monotonic decrease in J_c sets in for $H\|c$; while J_c increases up to H_{peak} and decreases at higher fields for $H\|ab$. The range of the stochastic behavior in $J_c(H\|ab)$ expands and H_{peak} shifts to higher field as the temperature decreases. At 40 K, H_{peak} appears at 1.5 T and J_c is 60% higher than the
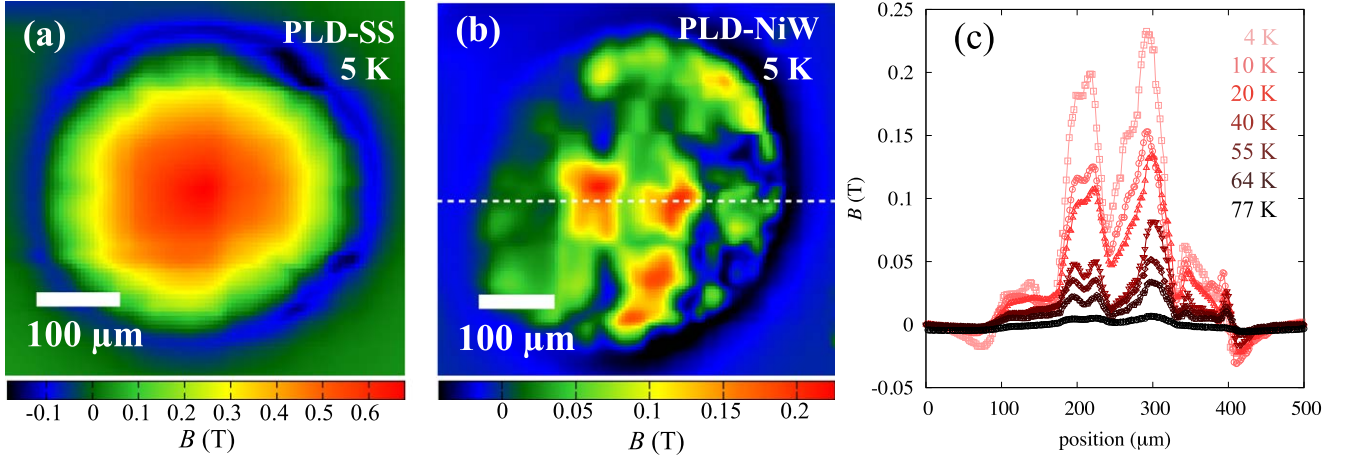
Figure 1. Remanent field maps of (a) PLD SS and (b) PLD NiW at 5 K. (c) Remanent field profile for PLD NiW at different temperatures corresponding to the position marked by the white dashed line in (b).
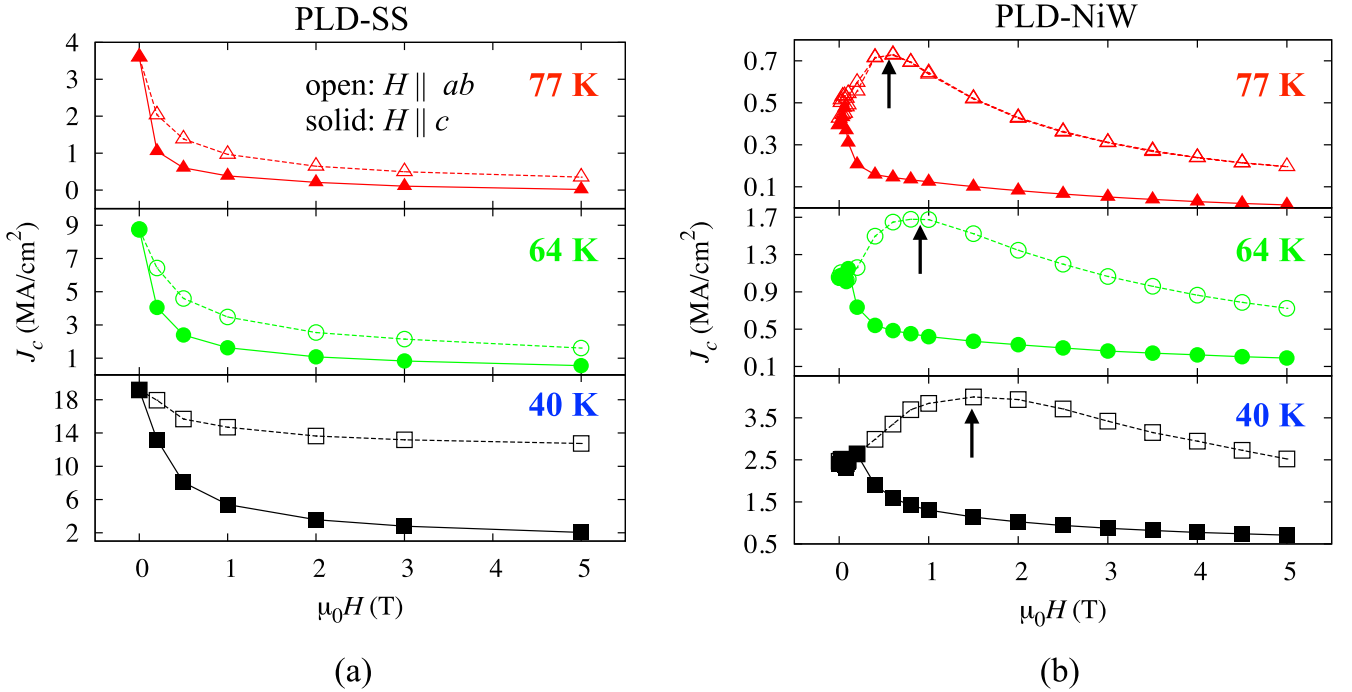
Figure 2. Field dependence of J_c of (a) PLD SS and (b) PLD NiW at temperatures of 40, 64 and 77 K in two orientations: $H\|ab$ (open symbols) and $H\|c$ (solid symbols). The black arrows denote the peak in $J_c(H\|ab)$ that shifts to higher fields with decreasing temperature.

self-field J_c at this temperature. Overall, the PLD-SS sample has about nine times larger J_c than PLD-NiW.

As can be observed in figure 3(a) where $J_c(H)$ at 64 K is plotted for increasing and decreasing magnetic fields, the peak in $J_c(H\|ab)$ occurs both in the increasing and decreasing branch and a small hysteresis is found around the peak. The difference in J_c between the increasing and decreasing field branch decreases as the field increases and disappears for fields oriented parallel to the c-axis. When the applied field is rotated towards the c-axis (figure 3(b)), H_{peak} shifts to lower fields until it disappears near $H\|c$. It is also worth noting that the slope of the increasing J_c part is the same at all angles. The inset shows the low field region where J_c fluctuates

stochastically up to 0.1 T and starts to increase for $\theta \geqslant 80°$ and to decrease for $\theta \leqslant 65°$.

At 40 K where the field of 0.2 T is roughly in the range where the stochastic behavior occurs and indicated by the red line in figure 4(a), J_c (red and circular data points in figure 4(b)) is almost angle-independent, and its value is close to the self-field J_c at this temperature. As the field is increased to 0.5 T (orange and inverted triangle points in figure 4(b)), the angle-independent J_c is confined to a range $\Delta\theta_{\text{GB}}$ of about 40° around $H\|ab$. J_c increases with field around 0.5 T for $H\|ab$. For applied fields of 1 T and above, J_c has its usual anisotropic behavior with a peak when the field is parallel to the ab-planes.
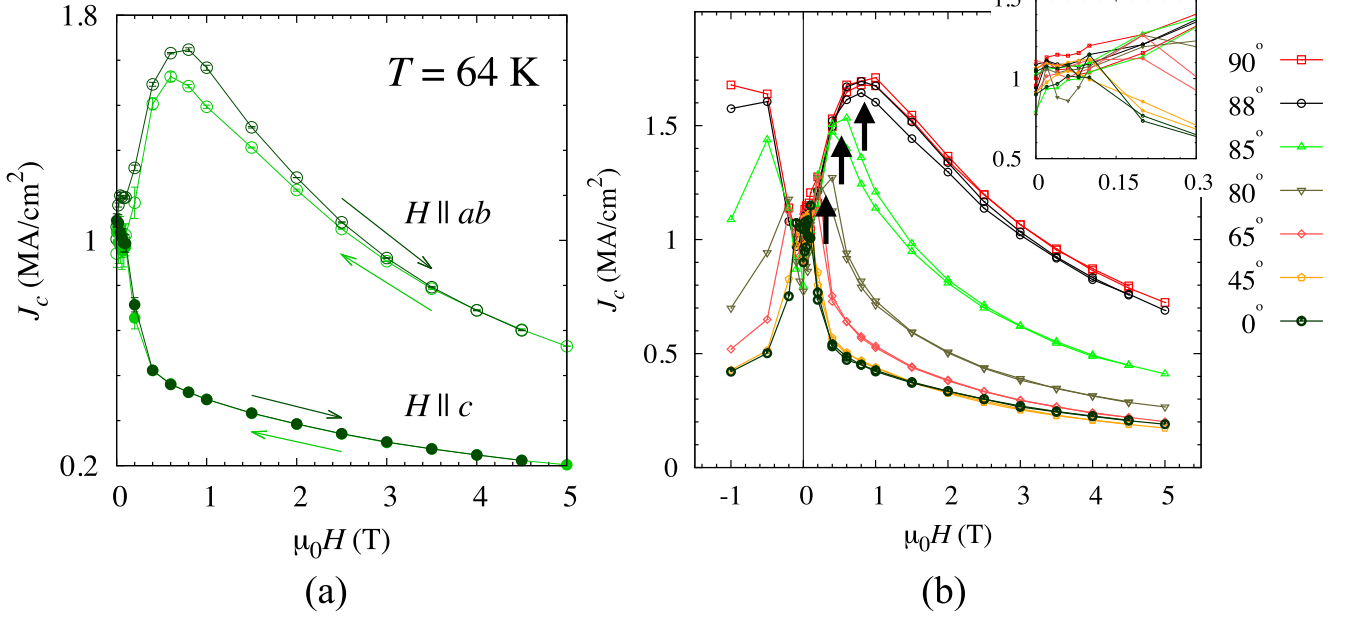
Figure 3. $J_c(H)$ of PLD NiW at $T = 64$ K for (a) increasing and decreasing field and (b) different angles between the applied field and the c axis. The inset shows the low field region.
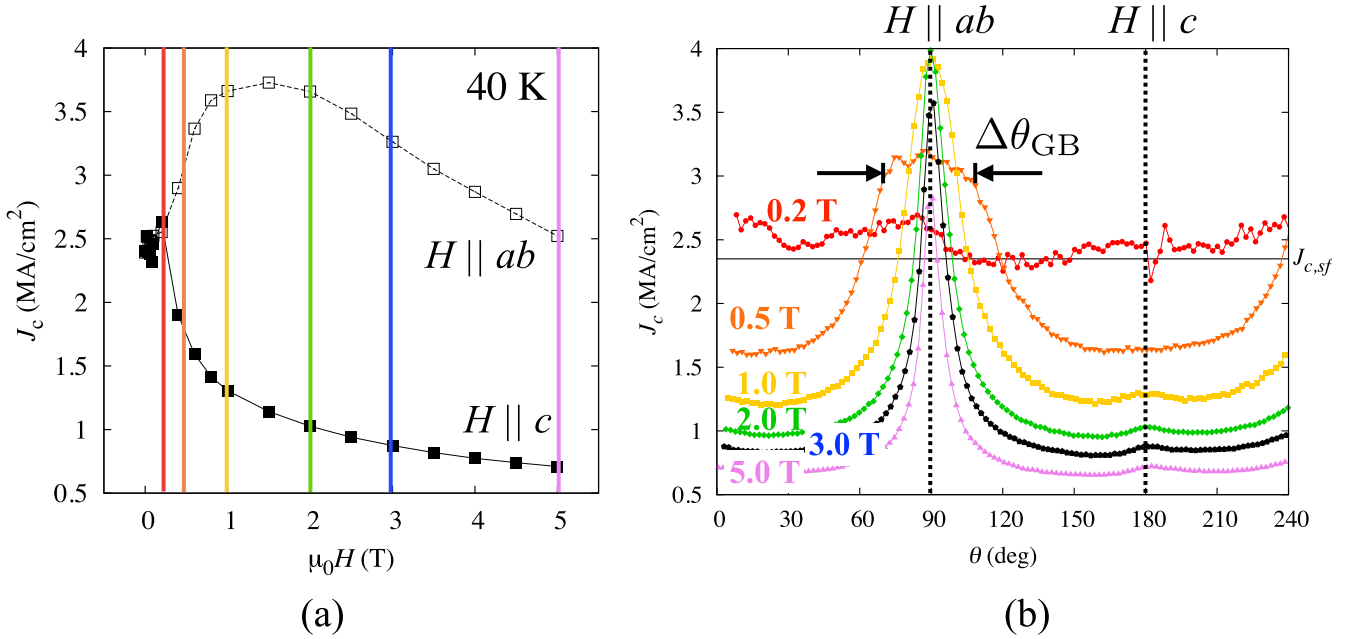
Figure 4. (a) Field dependence of J_c for PLD NiW at 40 K and in the main field orientations. The colored lines correspond to the fields of $J_c(\theta)$ curves in (b). (b) Angular dependence of J_c in different applied fields at 40 K. The black horizontal line indicate the self field J_c.

3.3. Non-monotonic field dependence of J_c

The granularity of the field profile of PLD-NiW is complemented by a peculiar behavior of the transport $J_c(H)$. Therefore, it is tempting to attribute the observed effects in J_c to the granularity of PLD-NiW. The appearance of a peak in $J_c(B)$ has been reported frequently. One scenario is due to electromagnetic granularity in YBCO films. Palau *et al* observed a peak in the decreasing field branch of the irreversible magnetization [11]. They attributed this peak to a minimum field at the GB when the applied field and the return field induced by the magnetic induction in each grain roughly compensate each other. The reduced field at the GB in turn raises the intergrain current density. Gapud *et al* reported this as well for transport measurements [12]. However, this interpretation depends on the history of the applied field and a peak would only occur in the decreasing field branch. Therefore, the model does not explain our transport data of PLD-NiW.
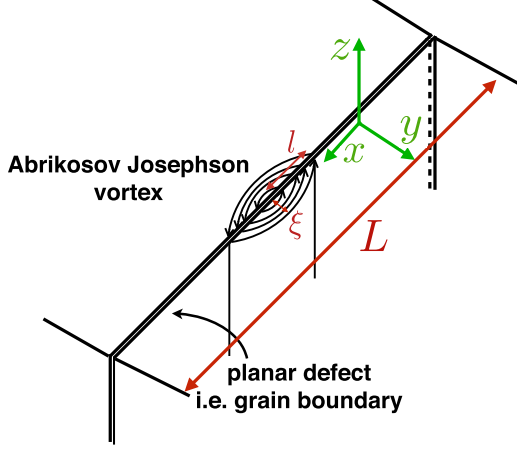
Figure 5. Representation of an Abrikosov Josephson vortex in a planar defect along the *xz* plane.

A plausible mechanism for the non-monotonic $J_c(B)$ in PLD-NiW was proposed by Gurevich and Cooley [13]. The model considers the magnetic interaction between AV and vortices residing in planar defects. A network of LAGBs is a perfect example for this system since it consists of an array of dislocation cores and strained superconducting channels that leads to suppression of the superconducting order parameter [14]. In addition, the GBs in PLD-grown YBCO are known to be planar [15]. LAGBs cause a distortion of the circulating current of a vortex lying in the boundary. Using the non-local Josephson equations which account for a local variation of the phase φ across a planar defect, Gurevich [13, 16] derived the field distribution for an AV interacting with the defect.

Consider a vortex lying in a GB as illustrated in figure 5. It is predicted to have a length l parallel to the planar defect (parallel to the *x*-axis), which is larger than its coherence length, ξ, perpendicular to the defect (parallel to the *y*-axis). Such a vortex is referred to as an AJV. Therefore, an AJV experiences weaker pinning parallel to a planar defect due to its larger dimension along this direction. Two contributions are considered for the pinning force on an AJV. One arises from inhomogeneities along the planar defects, the other from the effective interaction between the AJV and the AVs pinned in the grains. The total pinning force per unit length is [13]:

$$f_{\mathrm{GB}} = \frac{\Phi_\circ^2}{16\pi^2\mu_\circ\lambda^2}\left(\frac{\alpha L}{L^2 + l^2} + \sqrt{\frac{B}{\pi\Phi_\circ}}\right), \tag{1}$$

where L is the length of the inhomogeneity (see figure 5), α characterizes the degree of inhomogeneity in the GB, $\Phi_\circ$ is the flux quantum, $\mu_\circ$ is the vacuum permeability and λ is the penetration depth.

In the single-vortex approximation, the critical current density perpendicular to a planar GB, J_c^{GB}, can be obtained by balancing f_{GB} with the product of J_c^{GB} and a single flux quantum. Therefore, $J_c^{\mathrm{GB}}(B)$ can be expressed as

$$J_c^{\mathrm{GB}}(B) = J_\circ\left(1 + \sqrt{\frac{B}{B_s}}\right), \tag{2}$$

where

$$J_\circ = \frac{\Phi_\circ^2}{16\pi^2\mu_\circ\lambda^2}\left[\frac{\alpha L}{\Phi_\circ(L^2 + l^2)}\right], \tag{3}$$

$$B_s = \pi\Phi_\circ\left[\frac{\alpha^2 L^2}{(L^2 + l^2)^2}\right]. \tag{4}$$

Hence, the field range in which J_c of the PLD-NiW sample increases is attributed to the described mechanism of AJVs in the GB being pinned by the adjacent AVs and inhomogeneities and is therefore considered as GB-limited. Above H_{peak}, the limitation of J_c is given by vortex depinning within the grains. The observed decrease of J_c with B in the pinning-limited regime is described by the modified Kim model [17] for sufficiently small fields (i.e. much less than the irreversibility field):

$$J_c^{\mathrm{G}}(B) = J_{c0}\left(1 + \frac{B}{B_\circ}\right)^{-\beta}. \tag{5}$$

Equation (2) was fitted in the field range of increasing J_c while equation (5) was fitted above H_{peak} as shown for three temperatures in figure 6. The fitting parameters are given in table 1.

The parameters $J_\circ$ and B_s defined by equations (3) and (4) both depend on the characteristics of the GB. B_s is interpreted as the field at which shear flux pinning becomes dominant for f_{GB}. The parameter $J_\circ$ refers to the current density at $B = 0$ if the mechanism is purely determined by AJ flux lines penetrating along the GB. However, there is a discrepancy between the values of $J_\circ$ and experimental data with $J_c(H = 0)$ as shown in figure 6. At very low fields, the stochastic variation in J_c is probably due to strong percolation of currents within the network of grain and GB as a statistical ensemble [18]. The values of the exponent β in equation (5) are within typical values reported for different CCs in the pinning-limited regime [19].

The magnetic penetration depth λ can be calculated by using equations (3) and (4). The values obtained at 40 K, 64 K and 77 K are 155 nm, 197 nm and 273 nm, respectively and are denoted here as λ_{calc}. The penetration depth is known to have the following temperature dependence:

$$\lambda(T) = \lambda(0)\left[1 - \left(\frac{T}{T_c}\right)^b\right]^{-\frac{1}{2}}. \tag{6}$$

Thus, with the set of λ_{calc}, $\lambda_{\mathrm{calc}}(0)$ and b are calculated to be 133 nm and 1.7, respectively. For a *d*-wave superconductor, b takes a value of $4/3$ [20] while $\lambda(0)$ is generally difficult to determine. Literature values of $\lambda(0)$ for YBCO range between 115 and 130 nm [21–23]. Therefore, the values of λ_{calc} and the fitting parameters, $\lambda_{\mathrm{calc}}(0)$ and b are within an acceptable range.

Since the appearance of a peak in $J_c(H)$ of PLD-NiW at $H\|ab$ shows a transition from a GB-limited regime to grain-limited regime, B_{peak}, which is related to H_{peak} as, $B_{\mathrm{peak}} = \mu_0 H_{\mathrm{peak}}$, can be interpreted as the field at which J_c^{G} is
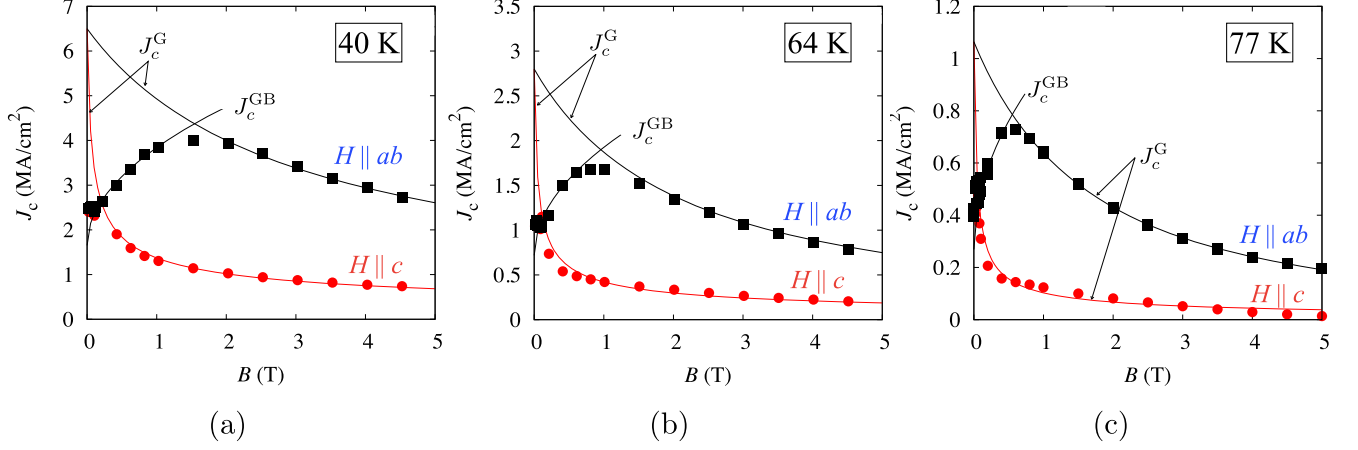
Figure 6. Field dependence of J_c for PLD NiW in main field orientations at (a) 40 K, (b) 64 K and (c) 77 K. The symbols correspond to the experimental data while the solid lines are fits by equations (2) and (5).

Table 1. Parameters for the fits of $J_c^G(B)$ and $J_c^{GB}(B)$ at 40, 64 and 77 K.

T (K)	B_s (T)	J_o (MA cm^{-2})	$J_c(0)$ (MA cm^{-2})	$B_o[\|c]$ (T)	$B_o[\|ab]$, (T)	$\beta[\|c]$	$\beta[\|ab]$
40	0.56	1.60	6.50	0.03	2.61	0.44	0.85
64	0.35	0.71	2.80	0.03	2.50	0.47	1.20
77	0.15	0.27	1.06	0.02	2.76	0.62	1.66
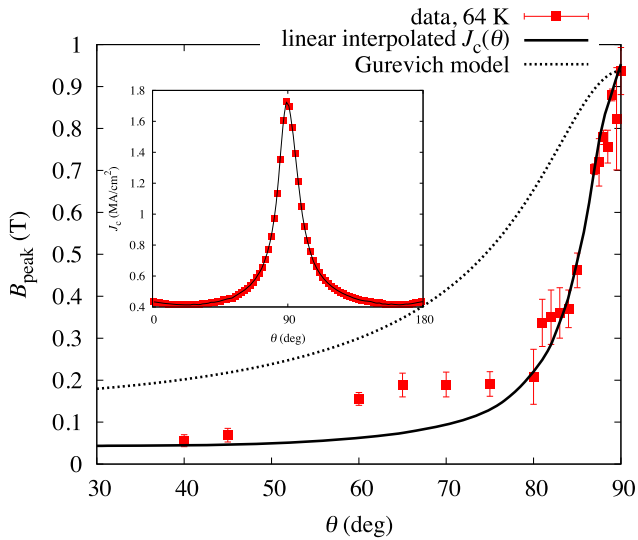
Figure 7. Dependence of B_{peak} on the angle θ. The data points are experimental values and the lines are those predicted using linear interpolation (black) and the Gurevich Cooley model (dashed blue). The inset corresponds to the experimental data of $J_c(\theta)$ at 64 K and 1 T with the linear interpolation.

approximately equal to J_c^{GB}. Therefore, J_c^G can be equated to equation (2) and B_{peak} can be expressed as

$$B_{peak}(\theta) \sim B_s \left(\frac{J_c^G(\theta)}{J_o} - 1 \right)^2. \tag{7}$$

As follows from equation (7), B_{peak} is directly related to J_c^G. Since J_c^G is anisotropic with respect to the direction of the applied magnetic field, it is expected that B_{peak} shifts towards smaller field as the field turns towards the c-axis direction. This is indeed the case for the experimental data in figure 3(b). The increasing segment in the field dependence of J_c merges into one curve while the onset of the intra-grain dominated field range decreases rapidly when the tape is tilted out of the field direction. This means that B_s and J_o are constant even if the direction of the applied field is varied around the GB. The parameters characterizing the inhomogeneities, α and L may be constant as well. Therefore, in the simplest case, the shift of B_{peak} with θ is influenced by the anisotropy of J_c^G for a given GB.

The function $B_{peak}(\theta)$ proposed in equation (7) can be compared to experimental data from figure 3(b) if an anisotropic $J_c^G(\theta)$ is assumed. A curve was fitted to the experimental data by linear interpolation to account for the rapid increase of J_c towards the ab-planes (inset in figure 7). According to the Gurevich Cooley model, the increase in $J_c(B)$ occurs as long as $H_{c1} \ll H < H_d$, where H_d refers to the field at which the AJVs overlap: $H_d \sim \frac{\Phi_o}{l^2} \sim \left(\frac{J_c^{GB}}{j_d} \right)^2 H_{c2}$, where j_d is the depairing current density and H_{c2} is the upper critical field which is angle-dependent. Cantoni *et al* [24] have pointed out that B_{peak} in $J_c(B)$ agrees with the value of H_d. With this interpretation, the angular dependence of H_d would be dominated by the anisotropy of H_{c2}. However, as shown by the blue dashed curve in figure 7, such a dependence deviates from the steep decrease of H_{peak} near the
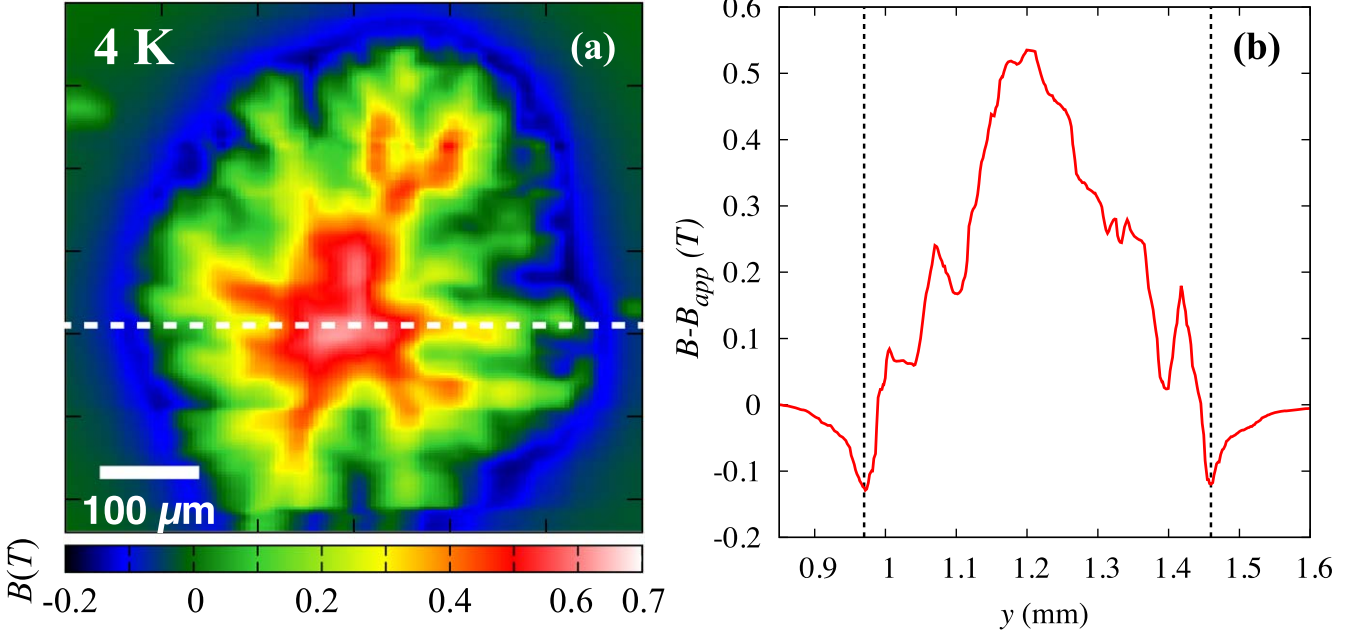
Figure 8. (a) Remanent field map of CSD NiW at 4 K. (b) Cut from the field map in (a). The black dashed lines indicate the sample edges.
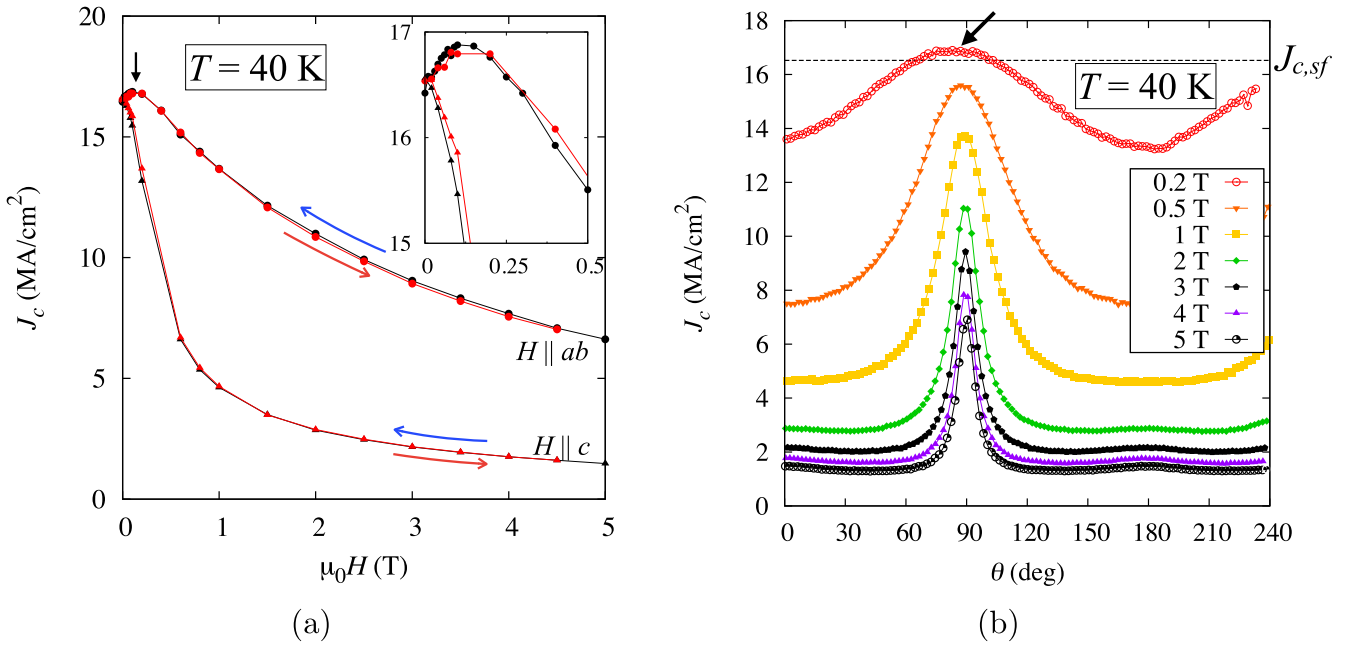
Figure 9. (a) Field dependence of J_c of CSD NiW at 40 K in the two main field orientations. The inset shows an enlarged view of the peak at low fields. (b) Angle dependence of J_c at 40 K and different applied fields. The dashed line indicate the self field J_c.

direction of the *ab*-planes and it is probably more suitable to use the irreversibility field in this case instead of H_{c2}. On the other hand, the $J_c(\theta)$ obtained by linearly interpolated curve fitting leads to a better agreement to the experimental data and the sharpness of the *ab*-peak is accounted. Note that the a curve was fitted to $J_c(\theta)$ at 1 T. At lower fields, the *ab*-peak usually becomes broader and this explains the deviation of the experimental data with B_{peak} of approximately 0.2 T and below to the $B_{\text{peak}}(\theta)$ predicted from the fit. An important implication of these results is that the good agreement between the data and the behavior of $B_{\text{peak}}(\theta)$ derived from

the fit to $J_c(\theta)$ demonstrates that the appearance of the peak in $J_c(B)$ is a consequence of the transition between the GB-limited regime, where the increasing J_c is governed by the dynamics of flux lines in the GBs and the grain-limited regime where the limitation of J_c is due to the vortices in the grains. The peak in $J_c(B)$ shifts to higher fields as H approaches the direction of the *ab*-planes because J_c^G decreases more slowly with increasing field than for $H\|c$. Such a GB-limited J_c at an angular range near the *ab*-plane direction was also reported by Horide *et al* in a YBCO film on a bicrystal substrate [25].

3.4. Granularity effects in CSD-grown YBCO on NiW

The YBCO film grown via CSD route has a different GB structure compared to the planar form resulting from PLD. The GB in CSD films are known to be meandering across the thickness of the YBCO layer which was already shown to suppress granularity effects on the transport J_c [26, 27]. Figure 8(a) shows the remanent field map of the CSD-NiW sample at 4 K. As seen further in the cut across the center of the map in figure 8(b), the granularity in the field profile is greatly suppressed, which appears only as peaks superimposed on an envelope depicting a global J_c.

Such a suppression of granularity has a corresponding manifestation in the transport J_c. The peak in $J_c(B)$ for $H\|ab$ is shifted to much lower fields, i.e. 0.12 T at 40 K, as shown in figure 9(a) while a monotonic decrease is observed for $H\|c$. No θ-independent range is observed in the angular dependence of J_c as in PLD-NiW, only a broad peak around the ab-plane direction is found at 0.2 T which slightly exceeds the self-field J_c as indicated by the arrow in figure 9(b). In addition, the J_c values of CSD-NiW and PLD-SS are comparable and much higher than in PLD-NiW.

The consistent suppression of granularity in magnetic field mapping and transport measurements in CSD-NiW further confirms that the peculiar behavior of the transport J_c with field is indeed related to granularity effects. The enhanced current transport between grains in CSD-NiW results from the meandering GBs that improve pinning of the AJ vortices and reduce current percolation which would lead to a scattered J_c at low fields. Therefore, J_c is limited by pinning in the grains in CSD-NiW in a wider field range than in PLD-NiW.

4. Conclusions

The effects of a granular morphology on J_c of CCs were revealed by transport measurements down to a temperature of 40 K. The magnetic field profiles obtained by SHPM have shown that J_c in PLD-YBCO on a stainless steel template with textured buffer layer is more homogenous than in PLD-YBCO on RABiTS NiW. In the corresponding field dependence of J_c, PLD-SS shows the usual monotonic decrease of J_c with increasing field while a peculiar behavior is observed in PLD-NiW. A peak in $J_c(B)$ appears when the field is oriented parallel to the ab-planes in PLD-NiW which shifts to higher field as the temperature is decreased. Such a peak appears at an applied field as high as 1.5 T at 40 K with J_c reaching twice of the self-field J_c at a given temperature. The critical current in the field range below the peak is grain-boundary limited where the increase in J_c can be explained by the physics of AJV lying in the GB as initially proposed by Gurevich and Cooley. An intra-grain pinning-limited regime prevails above the peak. The peak in $J_c(B)$ is likely to appear even at larger fields at lower temperatures. However, by choosing the CSD route for the growth of the YBCO layer on RABiT NiW, the effects of granularity are reduced, which is evident in the morphology of the field maps and the peak in the transport $J_c(B)$ occuring at a lower field of 0.13 T at 40 K.

References

[1] Verebelyi D T *et al* 2000 *Appl. Phys. Lett.* **76** 1755 7
[2] Hilgenkamp H and Mannhart J 2002 *Rev. Mod. Phys.* **74** 485 549
[3] Horide T, Matsumoto K, Yoshida Y, Mukaida M, Ichinose A and Horii S 2008 *Phys. Rev.* B **77** 132502
[4] Heinig N F, Redwing R D, Nordman J E and Larbalestier D C 1999 *Phys. Rev.* B **60** 1409
[5] Fernandez L, Holzapfel B, Schindler F, de Boer B, Attenberger A, Hänisch J and Schultz L 2003 *Phys. Rev.* B **67** 052503
[6] Lao M, Hecher J, Pahlke P, Sieger M, Hühne R and Eisterer M 2017 *Supercond. Sci. Technol.* **30** 104003
[7] Pahlke P, Sieger M, Chekhonin P, Skrotzki W, Hänisch J, Usoskin A, Strömer J, Schultz L and Hühne R 2016 *IEEE Trans. Appl. Supercond.* **26** 7201505
[8] Lao M, Hecher J, Sieger M, Pahlke P, Bauer M, Hühne R and Eisterer M 2017 *Supercond. Sci. Technol.* **30** 024004
[9] Hecher J, Baumgartner T, Weiss J D, Tarantini C, Yamamoto A, Jiang J, Hellstrom E E, Larbalestier D C and Eisterer M 2016 *Supercond. Sci. Technol.* **29** 025004
[10] Nast R, Vojenciak M, Demencik E, Kario A, Ringsdorf B, Jung A, Runtsch B, Grilli F and Goldacker W 2014 *J. Phys.: Conf. Ser.* **507** 022023
[11] Palau A, Puig T, Obradors X and Jooss C 2007 *Phys. Rev.* B **75** 054517
[12] Gapud A A, Christen D K, Feenstra R, List F A III and Khan A 2008 *Supercond. Sci. Technol.* **21** 075016
[13] Gurevich A and Cooley L D 1994 *Phys. Rev.* B **50** 13563 76
[14] Feldmann D M, Holesinger T G, Feenstra R and Larbalestier D C 2008 *J. Am. Ceram. Soc.* **91** 1869 82
[15] Durrell J H and Rutter N A 2009 *Supercond. Sci. Technol.* **22** 013001
[16] Gurevich A 1992 *Phys. Rev.* B **46** 3187 90
[17] Xu M, Shi D and Fox R 1990 *Phys. Rev.* B **42** 10773
[18] Evetts J E 2004 *Supercond. Sci. Technol.* **17** S315
[19] Senatore C, Barth C, Bonura M, Kulich M and Mondonico G 2016 *Supercond. Sci. Technol.* **29** 014002
[20] Prozorov R and Giannetta R W 2006 *Supercond. Sci. Technol.* **19** R41 67

[21] Sonier J E, Brewer J H, Kiefl R F, Morris G D, Miller R I, Bonn D A, Chakhalian J, Heffner R H, Hardy W N and Liang R 1999 *Phys. Rev. Lett.* **83** 4156

[22] Sonier J E *et al* 2007 *Phys. Rev.* B **76** 134518

[23] Zimmermann P *et al* 1995 *Phys. Rev.* B **52** 541

[24] Cantoni C, Verebelyi D T, Specht E D, Budai J and Christen D K 2005 *Phys. Rev.* B **71** 054509

[25] Horide T, Matsumoto K, Yoshida Y, Mukaida M, Ichinose A and Horii S 2007 *Physica* C **463** 678 81

[26] Feldmann D M, Holesinger T G, Feenstra R, Cantoni C W Z, Rupich M, Li X, Durrell J H, Gurevich A and Larbalestier D C 2007 *J. Appl. Phys.* **102** 083912

[27] Dinner R B, Moler K A, Beasley M R and Feldmann D M 2007 *Appl. Phys. Lett.* **90** 212501